2003

Monitoring North Pacific Heat Content Variability: An Indicator of Fish Quantity?

Tokmakian, R.

Earth Interactions, Volume 7, Paper No. 13, 2003
http://hdl.handle.net/10945/43794

Monitoring North Pacific Heat Content Variability: An Indicator of Fish Quantity?

R. Tokmakian

Department of Oceanography, Naval Postgraduate School, Monterey, California

Received 10 December 2002; accepted final form 24 June 2003

ABSTRACT: Fields of modeled sea surface heights and temperatures are used to develop an algorithm to monitor the low-frequency heat content variability of the North Pacific's midlatitudes associated with regime shifts in the circulation patterns of the Alaskan and the California Currents. Data from altimetric and infrared satellites are then used to apply the method using observational measurements. The model shows that the midlatitude Pacific subsurface circulation variability is primarily due to large, low-frequency horizontal north–south gyre movement. The changes may also be due to large-scale atmospheric changes in wind patterns, local mixing, as well as internal dynamics. It is proposed that this type of monitoring might be useful to help with understanding the variability in fisheries.

KEYWORDS: Altimetry, Heat content, North Pacific

1. Introduction

The low-frequency variability of the ocean's circulation and its relationship to the variability of marine populations has been explored to the first order (McGowan et al., 1998; Schwing et al., 2000). In these papers, the author explored the relationship between the long period changes in sea surface temperature (SST) with

Corresponding author address: Dr. R. Tokmakian, Department of Oceanography, Naval Postgraduate School, Monterey, CA 93943.

E-mail address: robint@ucar.edu

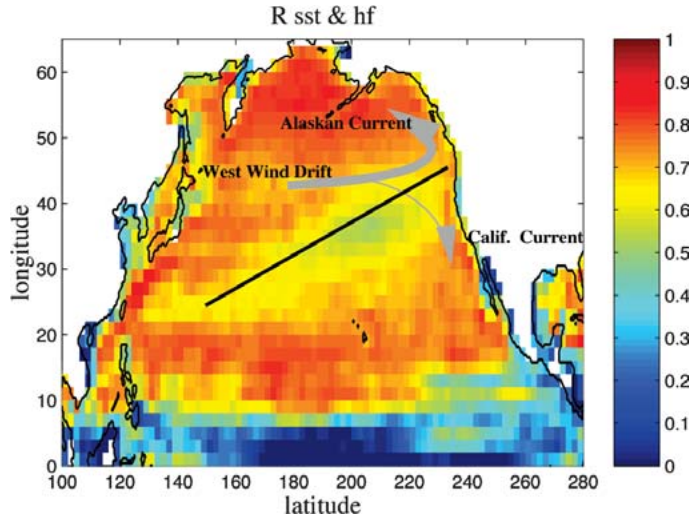

Figure 1. Correlation of the applied heat flux to SST of the model; low values are uncorrelated. The gray lines are a schematic of the currents. The weight of the gray lines indicate type; there is stronger northward flow for a type-B pattern. The black line is the transect for sampling the model and data.

disturbances in the coastal ecosystems. Large-scale interdecadal shifts of SST and atmospheric pressure are associated with a southward shift and intensification of the Aleutian low. Along with the atmospheric pressure shift is a shift in the location of the prevailing westerlies over the midlatitude central and eastern North Pacific. These shifts also cause changes in the sea surface height (SSH) field at a lower height corresponding to cooler, denser water below the surface, which may also reflect an increase in mixing of nutrient rich waters. These papers refer to two phases: "A," where the Aleutian low is shallow, and the central gyre ocean is relatively warm; and "B" with cool water and a deep Aleutian low. The basic circulation pattern of the northeast Pacific (McGowan et al., 1998) can be described as the North Pacific Current (West Wind Drift) flowing into both the Alaska Current system (cyclonic) and the California Current (Figure 1). The strength of the Alaska Current system is in phase with this fluctuation, while there appears to be no distinct phasing relationship with the California system. Here, we consider whether a space-based monitoring system can be developed to monitor and predict of the size of various fish stocks by watching the North Pacific heat content progress through these phases. This would be similar to how we monitor the tropical SSH pattern and its relation to changes in SST (Chambers et al., 1998).

The relationships between the marine populations, the ocean heat content, and the atmospheric conditions and their changes over time are illustrated in Figure 2. The marine populations are represented by the salmon catch off of Alaska and the heat content is represented by the changes in the height of the sea surface. The North Pacific (NP) index is representing the strength of the wind forcing. The NP index is defined by Trenberth and Hurrell (Trenberth and Hurrell, 1994) as the area-weighted sea level pressure over the region 30°–65°N, 160°E–140°W.

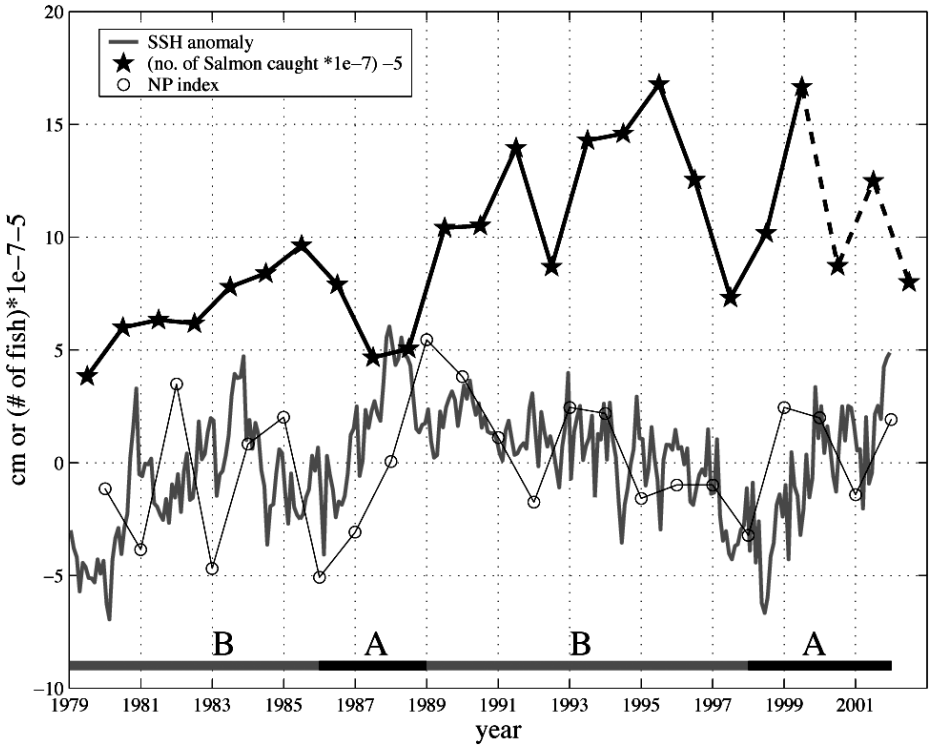

Figure 2. SSH anomaly signal at 35°N, 160°W (gray, thick line) compared to total salmon catch for Alaska (black line with stars). The numbers for 2000–02 (dashed line) are estimated or predicted. Also included on the plot is the NP index (thin, black line with circles). Salmon data are from National Marine Fisheries Service, Fisheries Statistics and Economics Division, Silver Spring, MD, and the Alaskan Department of Fish and Game (2002, personal communication). Here 2002 is a forecast; 2000 and 2001 are preliminary values.

The first half of the time series indicates a relatively large increase in the ocean's heat content at 35°N, 160°W in 1987/88 and may be connected to the large decrease in the fish catch. The last half of the record appears to be more strongly correlated with the atmospheric conditions than the first half. If these gyre changes to the ocean's heat content portend a trend in the fish catch in the northeastern Pacific, then monitoring the SSH low-frequency signal could be useful.

This paper discusses how an empirical technique of combining SSH anomaly measurements and SST measurements can be used to monitor the low-frequency change of heat content in the eastern North Pacific. Near-real-time measurements of satellite-derived SST [the Advanced Very High Resolution Radiometer (AVHRR) on the National Oceanic and Atmospheric Administration (NOAA) operational satellites; Smith et al., 1996] and altimetric-derived [TOPEX/Poseidon (T/P) and the European Remote Sensing (ERS) satellites; Koblinsky et al., 1998] SSH anomaly (SSH′, i.e., the sea surface's deviation from a 9+ yr mean)

measurements are used in combination to create a proxy heat content estimate. An eddy-permitting ocean model (Tokmakian and Challenor, 2000) is used to test the feasibility of the method and also to extend the time series back in time from the period when high quality altimeter measurements were available.

2. Surface observations

Along the subtropical convergence zone, the output of simulations (covering 20 yr, 1979–98) shows that the heat content and SST are uncorrelated with the applied heat flux variability, as given by the meteorological fields produced by the European Centre for Medium-Weather Forecasts (ECMWF; Figure 3). This same lack of correlation can be found with heat flux fields and SST as measured by space-based satellite infrared instruments. The uncorrelated region covers approximately a wedge-shaped area and is defined for the Pacific Ocean so that it begins in the west at a location at approximately 22°N, 140°E and broadens to the east covering, at 120°W, an area between about 30° and 42°N. Within this wedge SST is highly correlated with the heat content of the upper layers and with the upper steric height, for a given location and time and dominated by the seasonal cycle, defined as (Gilson et al., 1998)

$$\eta_s' = \frac{1}{\rho_0} \int_{-300}^{0} \rho dz, \tag{1}$$

where ρ is the density of the water, ρ_0 is the average density, and dz is the layer thickness.

The height quantity for the deeper water, η_{lower}', below 300 m is similarly calculated. In this area of the ocean where the influence of applied heat flux is reduced, it is the physical processes, rather than the heat flux, within the ocean (advection and mixing) that contribute mostly to the SSH variability signal. The relationship between the heat content and the surface height is explained in detail in Jayne et al. (Jayne et al., 2003). If the haline contribution is neglected, then

$$\eta_s' = \alpha \int_{-300}^{0} T'(z) dz, \tag{2}$$

where T' is the temperature anomaly at a given depth and α is the thermal expansion coefficient defined as

$$\alpha = \frac{1}{\rho_0} \frac{\partial \rho}{\partial T'}, \tag{3}$$

and is assumed to be constant with depth in this application. Further, Equation (2) can be expanded as

$$\eta_s' = \alpha T'(\text{at surface}) \Delta z + \alpha \int_{-300}^{\text{subsurface}} T' dz. \tag{4}$$

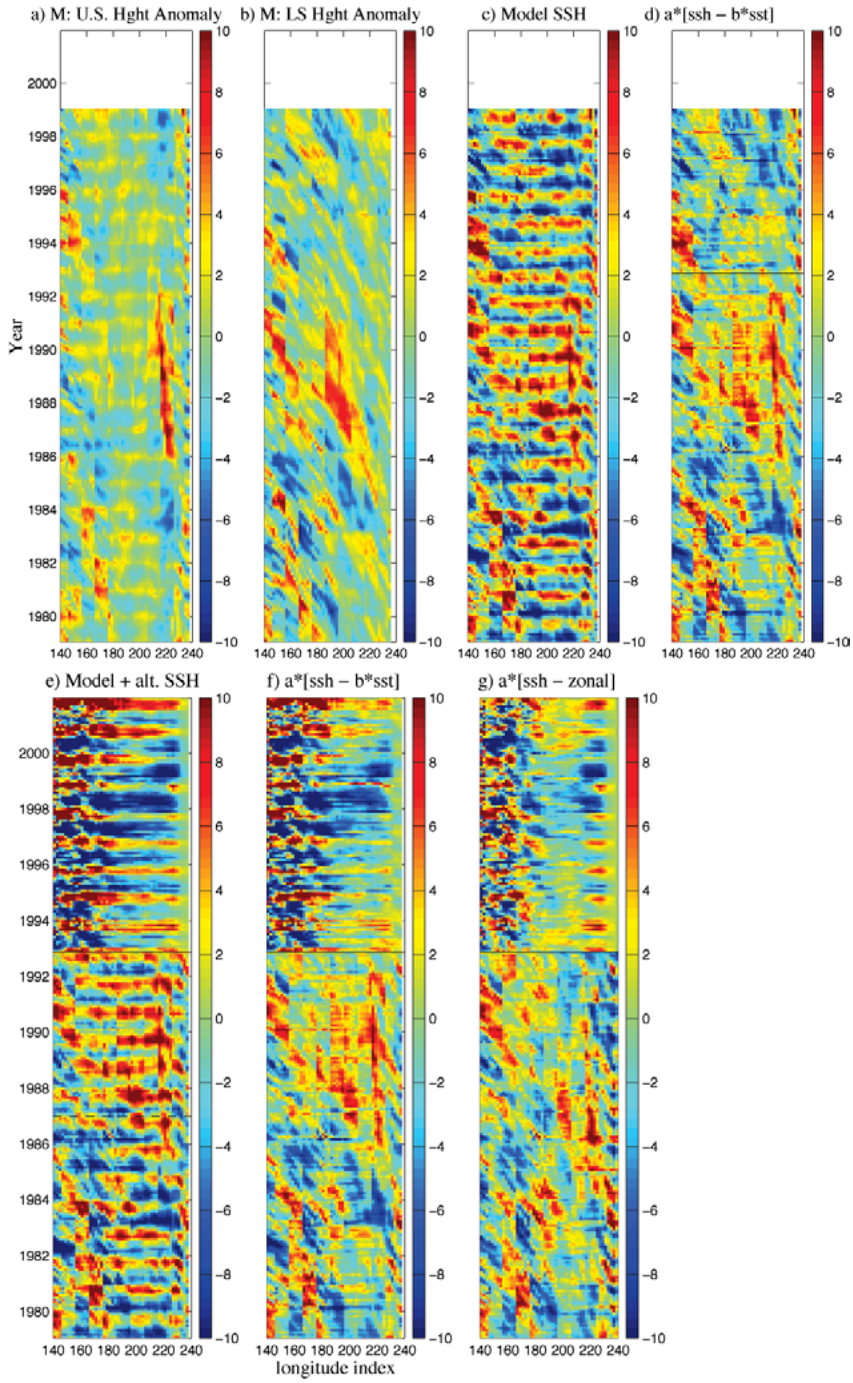

Figure 3. (a), (b), (c), (d) "Time–longitude index" plots of the time-varying anomalies of (a) upper steric height of model (0~300 m), (b) lower steric height of model (300 m at the bottom), (c) model SSH, (d) computed "proxy heat content" using model SSH + model SST such that α SSH′ $-$ β SST′. (e), (f) Same as (a), (b), except with altimeter data for 1992–2001; (g) same as (f), except with zonal SSH mean removed. Latitudes correspond to transect along the diagonal in Figure 1. Units are in centimeters.

The relationship between heat content (storage) and the upper steric height anomaly is defined at a location as

$$H' = \rho c_p \int_{-300}^{0} T'(z)dz, \tag{5}$$

if we assume that ρ and c_p, the density and heat capacity, change by less than 1%. Direct substitution, therefore, gives $H' = (\rho c_p/\alpha)\eta_s'$.

The low-frequency signal can be monitored by using a combination of remotely sensed measurements of SSH and SST. This signal is discussed, for example, in Zhang (Zhang, 1998) who notes the changes in the temperature field at 400 m and describes the decadal "seesaw" pattern in the midlatitudes and subtropics circulating in the North Pacific with a 20-yr period. We are proposing to monitor these integrated changes in the subsurface fields by using, as a proxy, an adjusted sea surface height field.

3. Testing the method using a model

To test this approach, the output from an eddy-permitting high-resolution (1/4° primitive equation ocean model; Tokmakian and Challenor, 2000) is used to create a proxy heat content field from the anomalies of the model's SSH and SST anomalies (SST′). The proxy field is then compared to the model's own estimate of η_s' and η_{lower}' to see how well it represents the low-frequency heat content signal in the subsurface layers of the ocean. In the example, the above quantities are extracted from the model fields along the transect shown in Figure 1. Figure 3 shows (a) η_s' and (b) η_{lower}', (c) SSH′, and (d) the estimate of the low-frequency variability.

Figure 3d, the proxy "heat content" field [see Equation (4)], is created by computing

$$\eta_s' = \alpha^*\text{SSH}' - \beta^*\text{SST}', \tag{6}$$

where α and β are the optimal values from a set that corresponds to the regression of SSH′ and SST′ on both η_s' and η_{lower}'. Physically, these coefficients represent the percentage of total signal that can be represented by either the SSH′ time series or the SST anomaly time series.

Figure 3a clearly shows the seasonal surface signal. The underlying interannual signal is difficult to detect, except for the especially strong "propagating" signal in the east between 1986 and 1990.

In Figure 3 the goal is to try to estimate the low-frequency signal of the ocean's heat content with real-time products through the removal of the changes in the near-surface seasonal signals. Optimal values are set at 0.6 for α and at 0.5 for β. Figure 3d can then be produced and shows corrected SSH anomalies in centimeters, rather than in units of heat content. The coefficients vary somewhat across the section, and average values are used rather than location-specific values. This is due to the fact that our model, although fairly realistic, does not represent the true relationships in the ocean.

The skill (correlation squared) of the model (also described as the percentage of

the variance explained in Figure 3b) used to explain Figure 3d is on the order of 0.6 (60%) for the points between 160° and 210°E. The section between 210° and 225°E is closer in its representation to Figure 3a, with the heat flux component removed (not shown), describing up to 80% of the variance. If it is assumed that there are 20 independent points (20-yr time series), then the SSH′ corrected series (Figure 3d) across the section are significantly ($\rho_{\text{critical}} = 0.44$, ρ is the correlation value) correlated with the lower portion of the water column. The section between 210° and 225°E is significantly correlated with the upper portion of the water column.

In the steric height field of the lower portion of the water column (Figure 3b), the unfiltered, monthly mean fields show many anomalies moving east to west, with a large increase in the height occurring midgyre, between the years 1987 and 1992. Figures 3c,d show the SSH monthly fields from the model with and without the correction considering the SST quantity. Figure 3c clearly shows the deeper interannual signal seen in Figure 3b. By examining the corresponding velocity vectors, the smaller spatial propagating signals are related to gyre movement north and south, while the large "warming" event is related to weaker winds in this region (seen in the model's momentum fields) and result in less deep mixing.

The model output clearly shows that with adequate sampling of SSH and SST from satellites, it is possible to monitor the low-frequency changes of the subtropical gyre, including changes in the deeper subsurface layers. First, west of 175°E (and, thus, below 25°N) the variability in the water column changes similarly for the upper and the deeper waters below 300 m.

Second, east of 175° and west of about 205°E (north of ~30°–35°N), the lower portion of the water column contributes most to the SSH variability. This is due to the strong influence of mixing to deeper levels and the variation of the winter mixing in different years. This strong, deep wintertime mixing is forced by the anomalously strong wind forcing, indicated by the NP index value in Figure 2 (thin black line with circles). The strong interannual variation in winter mixing extends farther north, but the model simulation shows in the section east of 205° and west of 225°E, that the upper ocean is the strongest contributor to the surface variability. This can be visually seen in Figure 3d between years 1986 and 1990 by the high anomaly feature that is stationary in space at 220°E. This feature may or may not be realistic, but in the model, this upper-ocean signal is due to the accumulation and some advection of heat in the upper layers of the model. And finally, at the eastern edge, both the upper and lower portions contribute equally to the surface height variability.

How realistic is it to use an SSH "corrected" by the satellite SST measurements in estimating the heat content of the subsurface layers? It has been suggested that the method is equivalent to removing the zonal mean of SSH from the SSH estimate. (Note: Removing the zonal mean of SST produces a similar plot to Figure 3d.) To understand the difference between removing the zonal SSH signal and removing the local SST signal, a plot similar to Figure 3d was produced and an analysis of the difference was done. The comparison shows that west of about 180° (and thus south of about 30°N), the two methods produce largely equivalent signals. East of 180° (and north of 30°N), the two methods diverge, reflecting that the heat content variability is not just a change in the steric component forced by the atmospheric heat flux alone. To illustrate the difference, Figure 4 shows a time

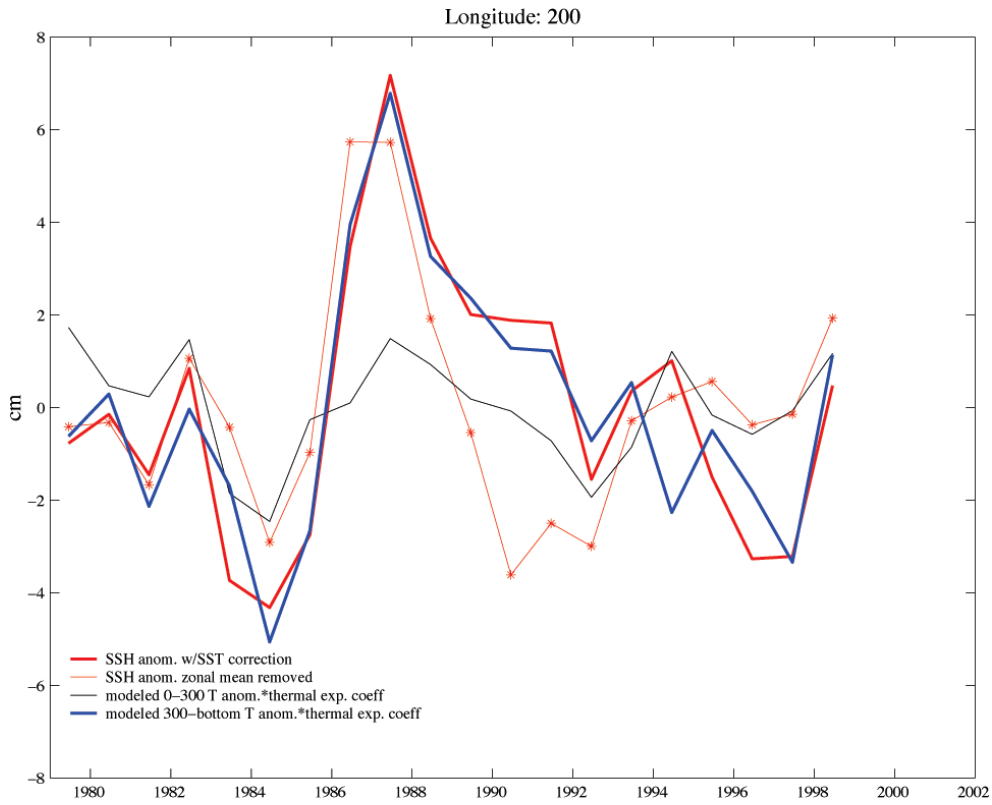

Figure 4. Estimated height change (red line) in subsurface layers of ocean estimated from model (1979–92) and altimeter SSH fields and SST data, estimated using SSH – zonal mean of SSH (red line with stars). The blue line with circles is the temperature anomaly (model output) below 300 m, and the black line with circles is the temperature anomaly (from model) 300 m and above.

series extracted along 200°E for the SSH quantity corrected by SST (heavy red line), the SSH with a zonal mean removed (thin red line with stars), the heat content of the upper layers (black line), and the heat content associated with the lower layers (blue line). The heat content series are multiplied by a thermal expansion coefficient to convert to units of centimeters. The figure shows that there are similarities and differences between the two red lines and how they reflect the heat content in the upper- and lower-model levels. The major differences exhibit themselves during the 1988–94 and 1996–98 periods. In the first period, the difference shows that the zonal mean removes the signal that relates to the deeper waters. The zonal mean removal technique shows a cooler ocean during the first period and a warmer ocean during the second period. The removal of the zonal SSH mean deletes a portion of the interannual signal that is of interest.

From detailed analysis of the time series at all longitudes consisting of computing regressions and correlations, it is found that the method that best

corrects SSH to reflect the heat content along the whole section uses the local SST values rather than a zonal mean SSH.

Next, the modeled SSH′ were replaced with satellite measured SSH′, the average of available T/P and ERS data (October 1992–2001). The modeled SST is replaced with AVHRR SSTs. The same adjustment to the SSH′ fields is made as described above. The resulting three plots are shown in Figures 3e (the model plus altimeter SSH fields), 3f (the adjusted model plus altimeter SSH fields using the SST correction), and 3g (the SSH field adjusted using a zonal SSH mean). The first portion (1979–92) of each plot is identical to Figures 3c,d and the rest (late 1992–2001) is the satellite data. For the latter portion of the record, it can be seen that the model fields are similar to what the satellites have measured. The difference between the plots with the SST correction and the zonal mean correction shows that removing a zonal mean SSH from each point results in a somewhat warmer ocean during the "cold" period centered around 1998/99.

4. Independent observations

To validate our estimates of changes in low-frequency heat content as measured by satellites, an independent, in situ dataset of ocean temperatures is compared to the proxy heat content. Available temperatures from ship observations, either CTD or XBT data have been incorporated into an online dataset maintained by NOAA's Pacific Fisheries Environmental Laboratory (PFEL). These data are provided via the PFEL, live access server, and are monthly means of Canada's Marine Environmental Data Service (MEDS) and other subsurface temperature observations received from NOAA's National Oceanographic Data Center (NODC). The temperature data have been averaged on a 1° latitude–longitude grid and interpolated to 19 standard depth levels. The following three datasets make up the database: 1) monthly real-time GTSPP (for the period 1999–2001); 2) best copy GTSPP (higher-resolution delayed-mode data that often duplicates or supersedes real-time profiles for the period 1991–98); and 3) World Ocean Data (Levitus; Conkright et al. 1998) for 1979–90. More data for a particular time period is incorporated into the database as time passes, resulting in less data for the recent past in contrast to 5 or 10 years ago. For the purpose of providing an independent validation of the technique to estimate heat content, an average temperature anomaly change is then calculated for the top 300 m and for the data available below 300 m.

Figure 5 shows the two time–longitude plots along the same diagonal as before, but now extracted for subsurface in situ temperatures. This independent dataset of subsurface temperatures shows that the eastern basin of the subtropical gyre is warmer after 1999 than between 1994 and 1999. The upper layers in Figure 3a clearly show the seasonal cycle that is seen in Figure 3 for the modeled fields for the period when the data was from the World Ocean Data (Levitus; Conkright et al. 1998) 1979–90. In the lower portion of the water column (Figure 3b), the model has replicated the change seen in the observations that appear to propagate from east to west (e.g., 1984–88). The observations also clearly indicate a cooling of the North Pacific in the east during the early 1990s with a tendency toward warming in 1999–2000 (similar to the altimeter estimates).

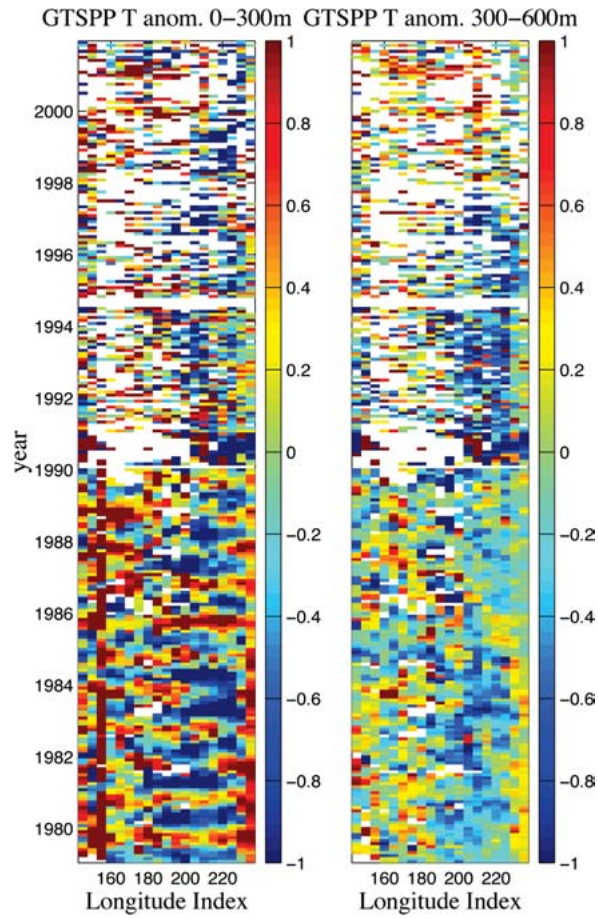

Figure 5. (left) Average temperature anomaly over top 300 m from GTSPP dataset, and (right) average temperature between 300 and 1000 m from GTSPP dataset (note some depths may be missing).

Figure 6 shows a similar time series to Figure 4 but with the modeled heat content replaced by the estimated fields from the data (Figure 5) and with the modeled SSH fields replaced from October 1992 with satellite-measured SSH (Figure 3f). We see that the satellite estimate appears to do a reasonable job with estimating the increase in the average temperature along 200°E. The plot also shows that the model contains a difference in an estimate of heat content between 1986 and 1990. This is the model failing to reproduce the observed low-frequency signal. After 1992, the SSH′ is from the signal observed by the altimeters. The altimeter derived low-frequency signal shows that it is reproducing qualitatively the change in heat content seen in the observations (a drop in heat content followed by a steep rise). The differences could be due to the sparse observational dataset available at this time as compared to the first half of the time series shown. For completeness, a third line, the thin red line with stars, represents the change in heat content along 200°E with a zonal SSH mean removed from the SSH signal (extracted from Figure 3g). This line produces a similar result, with 1998 showing

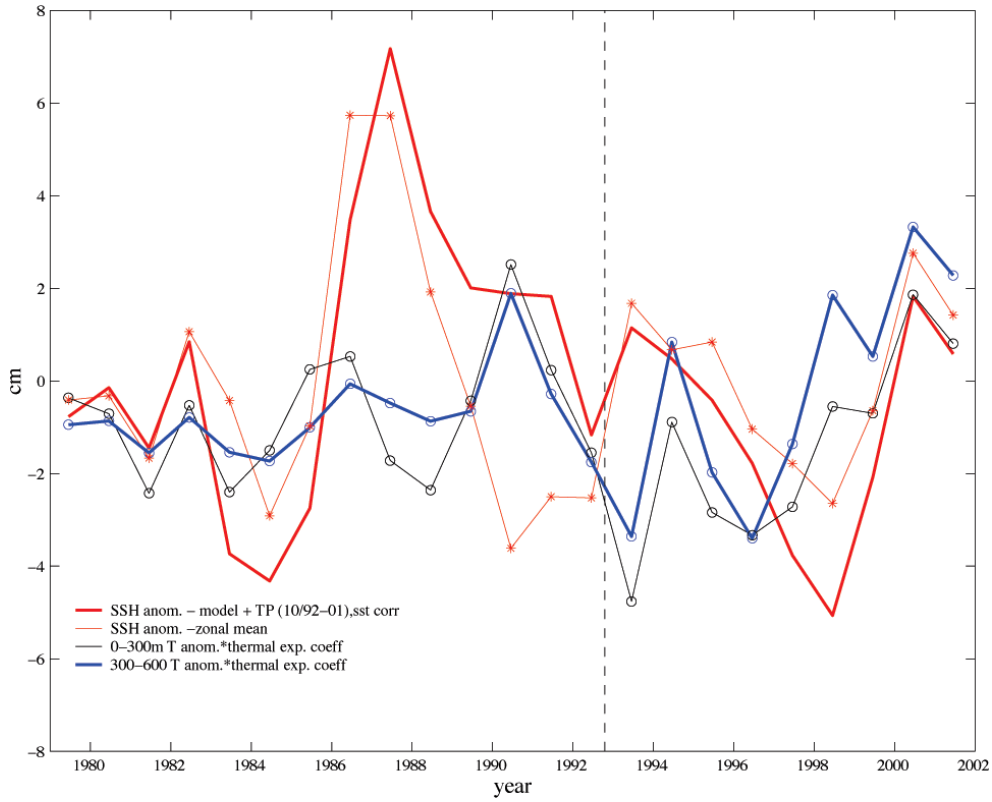

Figure 6. Estimated steric height change (red line) in subsurface layers of ocean estimated from model (1979–92) and altimeter SSH fields and SST data, the blue circles are mean anomaly temperatures below 300 m, and the black circles are 300 m and above. Samples are taken at 200°E, same as in Figure 4.

a warmer ocean than is calculated when just the SST signal is removed. Further investigations will be conducted to understand the usefulness of this estimate to both physical and biological oceanographers (including how this information might be useful to fishery science). A much longer time series of modeled fields, satellite data, and observational data is necessary to test the method further.

5. Discussion and conclusions

Through the use of the output from the four-dimensional ocean circulation model, we are able to explore further aspects of the circulation. Both coastal systems are significantly correlated with the variation in the North Pacific Current and its heat transport, with about 40% of the coastal flow prescribed by this large, low-frequency, North Pacific signal (correlations are on the order of 0.6–0.7). During the early portion of our modeled simulation (1980s), both the Alaskan Current and the California Current show a relative increase in their transports (a period of a strong Aleutian low and relatively low NP indexes, and a strong, warm Alaskan Current).

In contrast, the period between 1988 and 1989 shows relatively weaker flow in both directions. This middle period is the period with higher than average NP index values (relative to the period 1979–2002; Trenberth and Hurrell, 1994), indicating weaker mixing and warmer midgyre temperatures ("type-A" circulation pattern; McGowan et al., 1998).

In the late 1990s, the pattern returned to something similar to the early 1980s with generally strong westerlies and "type-B" circulation patterns. This is consistent with what Qiu (2002) found when looking only at the T/P data for the 1990s. Now in the 2000s, the westerlies have weakened again (with an NP index relatively higher than the mid-1990s). Also, the midgyre SSH anomaly is positive through late 2001 and the coast region a cooler, type-A regime. On average, the flow northward during the early 1980s and late 1990s is relatively strong as compared to the early 1990s The temporal change in the strength of the flow to the south appears to also follow this same pattern, but it is modified by the El Niño signal.

To understand how the SSH anomaly information might be useful in predicting the available "fish catch" for a future year, the total salmon catch off of Alaska [the National Marine Fisheries Service, Fisheries Statistics and Economics Division, 2002, personal communication (more information available online at www.st.nmfs.gov/st1)] is compared with the low-frequency SSH anomaly in the middle of the gyre, seen initially in Figure 2. It is, also, a well-known fact that the Alaskan salmon catch time series is out of phase with the Washington/Oregon catch (Mantua et al., 1997). During the early 1980s the Alaskan catch, relative to our +20-yr time series, is low. The Alaskan catch begins to increase from the mid- to late 1980s into the mid-1990s, where it then fluctuates through the late 1990s into the 2000s. The midgyre, indicating a type-B pattern (early 1980s, 1990s), corresponds to a trend toward increasing the salmon catch in the Alaskan gyre. The series also reflects a slight drop in the fish catch during a short type-A phase at the end of the 1980s and then again in the 2000s. The estimated SSH anomaly signal from the midgyre region indicates that the central-northeast Pacific is significantly warming (higher SSH values) from late 1998 and continuing on into 2002. The type-A phase thus indicates cooler waters off the Alaskan coast and less nutrient rich water supply from the midgyre, and a weaker northward flow leading to a reduction in the stock available for catch. Off the Oregon and Washington coast, the salmon catch tends to fluctuate in the opposite sense.

In summary, an empirical technique that monitors the low-frequency changes in SSH and associated heat content along a transect in the North Pacific has been developed and tested using both simulated fields and space-based measurements. By comparing to in situ data, the paper shows that using SST fields to remove the surface signal in the upper heat content of the oceans is a reasonable way to estimate the changes in the strength of the midgyre of the North Pacific and might contribute to a better estimate of predicting fish catch in the northeast Pacific Ocean. The estimate of the SSH anomaly for the end of 2001 (Figure 3f) suggests that the trend is for a decrease in the salmon catch off of Alaska and an increase in the catch off of Oregon and Washington.

Acknowledgments. This work is funded by grants from NASA JSWT, DOE, and from NOAA GLOBEC (in the northeastern Pacific). Computer computations for model simulations

were provided by NCAR. Thanks to Koblinsky et al., for altimeter Pathfinder data, to JPL for AVHRR Pathfinder data (MCSST), and to PFEL (Lynn DeWitt). The author thanks the two reviewers for their time and the suggestion from one to look at how the method differs from a method that removes a zonal mean.

References

Chambers, D. P., B. D. Tapley, and R.H. Stewart, 1998: Measuring heat storage changes in the equatoral Pacific: A comparison between TOPEX altimetry and TAO buoys. *J. Geophys. Res.,* **103,** 18,591–18,597.

Conkright, E. M., and Coauthors, 1998: *World Ocean Database 1998 Data Set Documentation*. National Oceanographic Data Center, CD-ROM.

Gilson, J., D. Roemmich, and B. Cornuelle, 1998: Relationship of TOPEX/Poseidon altimetric height to steric height and circulation in the North Pacific. *J. Geophys. Res.,* **103,** 27,947–27,965.

Jayne, S. R., J. M. Wahr, and F. O. Bryan, 2003: Observing ocean heat content using satellite gravity and altimetry. *J. Geophys. Res.,* **108,** 3031, doi:10.1029/2002JC001619.

Koblinsky, C., et al., cited 1998: NASA/GSFC Ocean Pathfinder. [Available online at http://neptune.gsfc.nasa.gov/ocean.html.]

Mantua, N. J., S. R. Hare, Y. Zhang, J. M. Wallace, and R. C. Francis, 1997: A Pacific interdecadal climate oscillation with impacts on salmon production. *Bull. Am. Meteor. Soc.,* **78,** 1069–1979.

McGowan, J., D. Cayan, and L. Dorman, 1998: Climate–ocean variability and ecosystem response in the northeast Pacific. *Science,* **281,** 210–217.

Qiu, B., 2002: Large-scale variability in the midlatitude subtropical and subpolar North Pacific Ocean: Observations and causes. *J. Phys. Oceanogr.,* **32,** 353–375.

Schwing, F.B., T. Murphree, and P.M. Green, 2002: The Northern Oscillation Index (NOI): A new climate index for the Northeast Pacific. *Progress in Oceanography,* Vol. 53, Pergamon, 115–139.

Smith, E., et al., cited 1996: Satellite-derived sea surface temperature data available from the NOAA/NASA Pathfinder Program. [Available online at http://www.agu.org/eos_elec/95274e.html.]

Tokmakian, R., and P. G. Challenor, 2000: On the joint estimation of model and satellite sea surface height anomaly errors. *Ocean Modelling,* **1,** 39–52.

Trenberth, K., and J. Hurrell, 1994: Decadal atmosphere–ocean variations in the Pacific. *Clim. Dyn.,* **9,** 303–319.

Zhang, R.-H., 1998: Decadal variability of temperature at a depth of 400 meters in the North Pacific Ocean. *Geophys. Res. Lett.,* **25,** 1197–1200.